



The Misery Point cliff, Mayaguana Island, SE Bahamas: a unique record of sea-level highstands since the Early Pleistocene

Fabienne Godefroid¹ · Pascal Kindler¹  · Massimo Chiaradia¹ · Gyöngyvér Fischer¹

Received: 26 November 2017 / Accepted: 2 October 2018 / Published online: 25 October 2018
© Swiss Geological Society 2018

Abstract

We describe in detail a unique succession of Lower Pleistocene shallow-water carbonates exposed at the Misery Point sea cliff along the northern shoreline of Mayaguana Island (SE Bahamas). This km-scale outcrop comprises a record of seven past sea-level highstands that occurred between ca. 1.3 Ma and 125 ka ago, and reached relative elevations from 3 to possibly 14 m above modern sea level. Considering the tectonic stability of the Mayaguana platform in the Quaternary, the amplitudes of the recorded events could be fairly close to the corresponding glacio-eustatic changes, and thus provide calibration points for sea-level proxies derived from the deep-sea oxygen-isotope records and ice-sheet models. Moreover, our study traces the evolution of the Mayaguana bank over the past 1.3 million years, provides some insight on the birth of possibly the first island of the Bahamas archipelago, and emphasizes that the shift from bioclastic to oolitic-peloidal carbonates (i.e. the transition from the pre-Lucayan to the Lucayan limestones) occurred much later on this platform than on the northern Bahamian banks, which raises questions about the origin of this transition.

Keywords Carbonate sedimentology · Geochronological dating · Sea-level history · Pleistocene

1 Introduction

In the past 50 years, numerous studies have focused on the description and the precise dating of Quaternary coastal and reefal deposits worldwide in order to reconstruct the amplitudes and frequencies of eustatic sea-level changes. The specific aims of these studies have been diverse. Some authors have attempted to confirm (Mesollela et al. 1969) or challenge (Thompson and Goldstein 2005) the astronomical theory of climate change. Others have presented sea-level reconstructions from stable (Hearty and Kindler 1995; Neumann and Hearty 1996; Thompson et al. 2011; O’Leary et al. 2013), tectonically uplifted (Gvirtzman 1994; Pedoja et al. 2014) or subsident (Camoin et al. 2001) areas. Finally, in the context of anthropologically driven global warming, others have investigated the record of warmer-than-present episodes to obtain clues about future

climate (Burkle 1993; Hearty and Tormey 2017). With few exceptions (e.g. Pirazzoli et al. 1993; Murray-Wallace 2002; Pedoja et al. 2014), these investigations have unfortunately been limited by the shortness of the studied stratigraphic record of the Middle and/or the Late Pleistocene.

Here we present an account of relative sea-level (RSL) highstands going back to almost 1.3 Ma from the tectonically stable island of Mayaguana in the south-eastern Bahamas. This record has been derived from the examination of a sea cliff 2–13 m high and extending for about 1.5 km along the north coast of the island. Part of these data have already been presented in a preliminary paper (Kindler et al. 2011), but subsequent fieldwork and new core data (Fischer 2019) have significantly changed our vision of the geological evolution of Mayaguana, opening the way for a new interpretation of the studied exposure. Furthermore, these data are here complemented by additional geochronological analyses. The closeness of the diverse sea-level indicators (reef, beach, notch and cave) of different ages observed on this sea cliff greatly reduces potential distortions linked to differential tectonics and isostatic adjustment. Thus, due to the tectonic stability (Pierson 1982; Godefroid 2012) and geographic position of

Editorial handling: S. Spezzaferri.

✉ Pascal Kindler
Pascal.Kindler@unige.ch

¹ Department of Earth Sciences, University of Geneva, 13 rue des Maraîchers, 1205 Geneva, Switzerland

Mayaguana, our reconstruction of RSL fluctuations might be fairly close to eustatic changes, and could thus provide calibration points for proxies derived from deep-sea oxygen-isotope records (e.g. Lisiecki and Raymo 2005; Raymo et al. 2006), and provide further constraints to ice-sheet models (e.g. DeConto and Pollard 2016). In addition, this exposure on Mayaguana represents a unique opportunity to gather more information on the Early Pleistocene which allegedly embraced “super-interglacial” periods, characterized by intensified melting of polar ice sheets and concomitant substantial rises of sea level (Scherer et al. 2003; Pollard and DeConto 2009). Finally, this study gives an insight of the evolution of carbonate production on the Bahamian banks during this time interval.

2 Setting

Mayaguana Island is located in the south-eastern part of the Bahamas archipelago (Fig. 1) and represents the emerged portion of a small (53 × 10 km), E–W trending, carbonate bank. The island itself is relatively flat compared to its northern counterparts (e.g. Eleuthera, Cat). The main reliefs consist of eolianites of Middle and Late Pleistocene age (Godefroid 2012).

Mayaguana is located close to the boundary between the North American and the Caribbean tectonic plates. It is surrounded by several fault systems, which have probably played a major role in the evolution of this platform during the Neogene (Fig. 1; Godefroid 2012; Fischer et al. 2016). These systems include (1) the Fifteen-Twenty Fracture Zone to the North of the platform; (2) the Cauto-Nipe Fault, which originates in Cuba and likely extends between the Mayaguana and the Caicos platforms (Meyerhoff and Hatten 1974); and (3) the SFZ, or Sunniland Fracture Zone,

which crosscuts the Bahamian archipelago. The Mayaguana Bank is located at less than 50 km to the West of the intersection of the Cauto Fault and the SFZ (Fig. 1).

Contrary to some northern Bahamas islands (e.g. New Providence, Eleuthera, San Salvador), and probably because of its remoteness, Mayaguana has not been the subject of many scientific investigations. Actually, only three major studies pertain to the geology of this island. Cant (1977) made a first reconnaissance of the fossil coral reefs forming most of its rocky coasts. All these coral terraces were then attributed to the last interglacial period. Pierson (1982) studied a series of cores drilled in the southwestern part of the island. He recognized several types of shallow-water carbonates based on allochem composition and diagenesis. In these cores, the limit between the pre-Lucayan and the Lucayan limestones (i.e. between hard, skeletal rocks and soft, oolitic-peloidal deposits; Beach and Ginsburg 1980) occurs at depths between 8 and 10 m below the island surface and, in one core, coincides also with the boundary between dolostones and calcarenites. On other Bahamian banks, this limit occurs at a much greater depth (e.g. 34 m on San Salvador; Supko 1977; 63.8 m on Great Bahama Bank; Kenter et al. 2001). This change in carbonate production and petrography occurred between 3.6 and 2.6 Ma ago, depending on the platform, and has tentatively been correlated with the onset of glaciations in the northern hemisphere (Beach and Ginsburg 1980; McNeill et al. 1988, 1998; Manfrino and Ginsburg 2001). More recent contributions on Mayaguana were made by Kindler et al. (2008, 2011) and Godefroid (2012) who studied the surface geology of the whole island. These authors identified and mapped eight main lithostratigraphic units (Fig. 2). In particular, they discovered large outcrops of limestones and dolostones dating from the Miocene, the Pliocene and the Early Pleistocene on the north coast of the island. These units represent the oldest marine deposits exposed at the surface of the archipelago, and expanded the previous stratigraphic record of the Bahamas islands (Carew and Mylroie 1995a; Hearty and Kaufman 2000) by several tens of million years. The studied exposure shows deposits assigned to the Misery Point, the Owl’s Hole, and the Grotto Beach formations (Fig. 2; Godefroid 2012).

Despite its proximity to an active plate boundary, the Bahamas archipelago has long been considered to be only affected by slow subsidence caused by thermally induced sedimentary loading (Mullins and Lynts 1977; Carew and Mylroie 1995b). Nonetheless, Pierson (1982) observed that Bahamian banks subside at different rates, and identified the Mayaguana platform as the most stable one (subsidence rate < 5 m/Myr). Because of the occurrence of Lower Miocene outcrops along the north coast, Kindler et al. (2011) surmised that Mayaguana had probably been titled towards the South, possibly during the Middle Pleistocene.

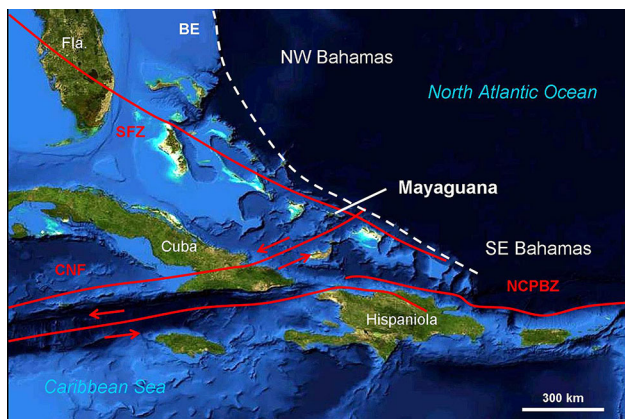
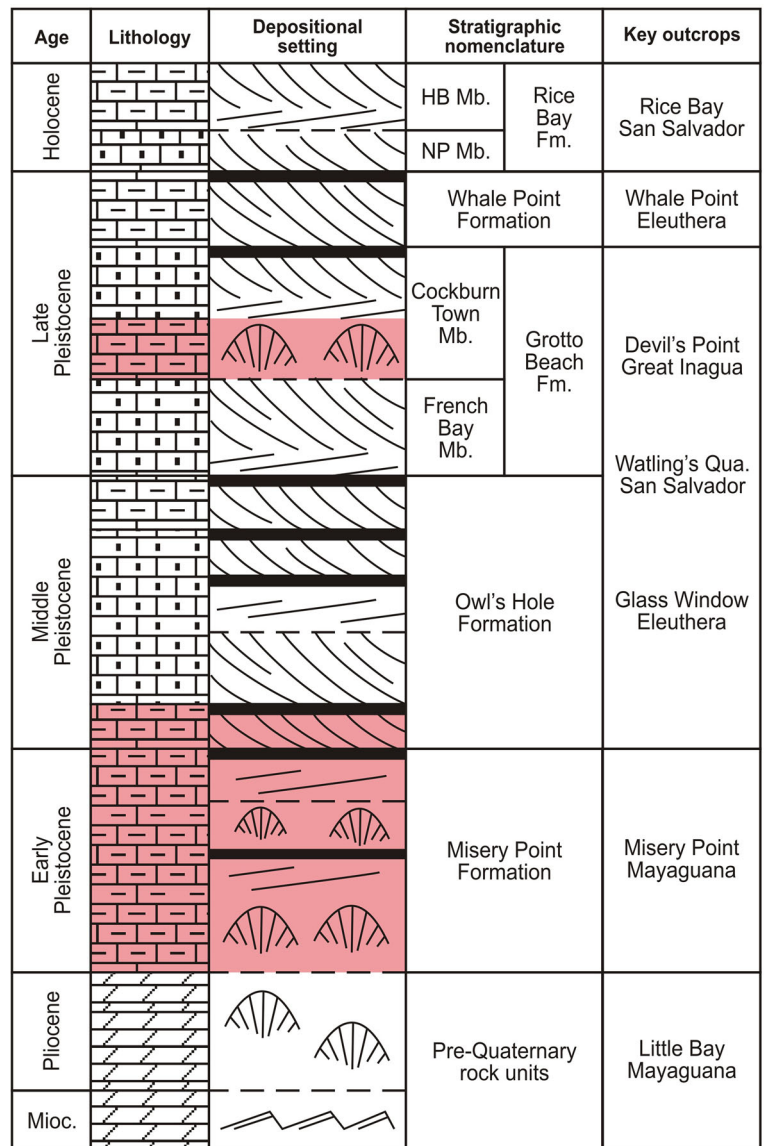
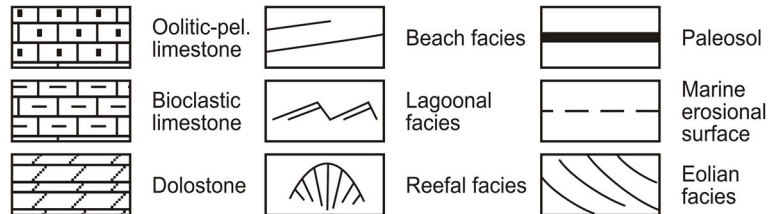


Fig. 1 Geographic and tectonic location of the Mayaguana Bank. Fla Florida; BE Bahama escarpment; SFZ Sunniland fracture zone; CNF Cauto Nipe Fault; NCPBZ North Caribbean Plate Boundary Zone. Background image from NASA

Fig. 2 Stratigraphy of the Bahamas islands (modified from Kindler et al. 2010). Highlighted intervals correspond to the rock succession exposed at the studied outcrop



LEGEND



However, this assumption has recently been invalidated by Fischer (2019) who found rocks of that age less than 2 m below the surface in the southern part of the island, i.e. at about the same height as the northern exposures. The present-day elevation (0 to +7 m) of these shallow-water carbonates (paleo-depth < 10 m) of Miocene and Pliocene age is consistent with the alleged sea-level stands during their accumulation. Indeed, because these former sea stands were most probably higher than the present one

(Miller et al. 2005), tectonic uplift needs not to be invoked to explain the actual position of these old rocks. In addition, since stratigraphic units occur here in vertical superimposition and do not exhibit a staircase arrangement as for example in Barbados (e.g. Speed 2012), Mayaguana has likely not experienced recent uplift. Based on data from Godefroid (2012), the maximal net subsidence rate since the Early Miocene can be estimated at 0.6 m/Myr (Fischer et al. 2016). The island could thus represent a close to

perfect gauge to record sea-level changes during the Quaternary.

3 Methods

3.1 Fieldwork

The sea cliff located to the West of Mount Misery Point (named hereafter the Misery Point cliff; Fig. 3) was examined on numerous occasions during the time span of the so-called Mayaguana Project (2007–2016). Fieldwork included sedimentological, paleontological and geomorphological examination of exposed rock units, and detailed stratigraphic logging. The thickness of stratigraphic units and the height of past sea-level indicators were measured with a tape, which was fairly easy on this vertical cliff. Measurement uncertainty is ca. ± 0.2 m. Physical and biogenic sedimentary structures, paleosols, unit boundaries, and dissolution features were minutely described. Samples were collected at depth with a hammer and chisel to minimize the effects of surface weathering.

3.2 Laboratory work

Fifty-six samples were gathered for petrographic studies with a light-transmitted microscope. Alizarine red-S and Feigl's solutions were used to identify dolomite and, respectively, aragonite in thin-section. Forty-nine powdered whole-rock samples, subsamples and corals were sent for mineralogical analysis and geochronological dating. The Sr-isotope, U-series, and amino-acid racemisation (AAR) techniques were used to date our samples. Details on sample preparation can be found in Godefroid (2012).

The $^{87}\text{Sr}/^{86}\text{Sr}$ ratio of seawater, and hence of precipitated marine carbonates, varies through time due to changes in continental erosion that provides ^{87}Sr , and in oceanic-ridge expansion, which delivers ^{86}Sr . The $^{87}\text{Sr}/^{86}\text{Sr}$ ratio of pure carbonate sediments of marine origin can thus be used for dating. In this paper, Sr separation and cleaning

procedures follow previously published methods (Horwitz et al. 1992). Some of the data were measured on a Nu instruments MC-ICPMS at IFM-GEOMAR (Kiel, Germany) in static mode. $^{87}\text{Sr}/^{86}\text{Sr}$ values were internally corrected for instrumental mass fractionation using an $^{88}\text{Sr}/^{86}\text{Sr}$ value of 8.375209. The external reproducibility (2σ) of the SRM987 standard was 27 ppm. Other Sr-isotope ratios were obtained on a Thermo TRITON mass spectrometer at the University of Geneva at a pyrometer-controlled temperature of 1480 °C on Faraday cups in static mode. Isotope measurements were carried out using the virtual amplifier design to cancel out biases in gain calibration among amplifiers. $^{87}\text{Sr}/^{86}\text{Sr}$ values were internally corrected for fractionation using an $^{88}\text{Sr}/^{86}\text{Sr}$ value of 8.375209. Raw values were further corrected for external fractionation by a value of +0.03‰, determined by repeated measurements of the SRM987 standard ($^{87}\text{Sr}/^{86}\text{Sr} = 0.710248$; McArthur et al. 2001). External reproducibility of the SRM987 standard was 7 ppm (1σ). Procedural blanks were < 100 pg Sr which is insignificant compared to the amounts of this element purified from the whole-rock samples. Other samples were recently measured using a Thermo Neptune PLUS Multi-Collector ICP-MS in static mode at the University of Geneva. The $^{88}\text{Sr}/^{86}\text{Sr}$ (8.375209) ratio was used to monitor internal fractionation during the run. Interferences at masses 84 (^{84}Kr), 86 (^{86}Kr) and 87 (^{87}Rb) were also corrected in-run by monitoring ^{83}Kr and ^{85}Rb . The SRM987 standard was used to check external reproducibility, which on the long-term (more than 100 measurements during 1 year) was 10 ppm (1σ). The internally corrected $^{87}\text{Sr}/^{86}\text{Sr}$ values were further corrected for external fractionation (due to a systematic difference between measured and a nominal standard ratio of the SRM987 of $^{87}\text{Sr}/^{86}\text{Sr} = 0.710248$; MacArthur et al. 2001) by a value of -0.023‰ per amu. Numerical ages were then obtained by comparison with the Sr-isotope evolution of global seawater for the Neogene reported in the look-up table Version 4:08/04 (Howarth and McArthur 1997; McArthur et al. 2001).

Selected coral and speleothem samples were sent for U-series measurements at IFM-GEOMAR. Element separation procedure, determination of U- and Th-isotope ratios, and age equations are described in Fietzke et al. (2005). We applied the same criteria as Blanchon et al. (2009) to assess the reliability of our dating results on coral samples: (1) the amount of diagenetic calcite must be less than 2%; (2) ^{238}U concentration values must range between 2.0 and 3.5 ppm; (3) ^{232}Th concentration values must be less than 2 ppb; (4) initial $^{234}\text{U}/^{238}\text{U}$ activity ratios must be comprised between $149 \pm 8\text{‰}$.

Amino-acid racemisation (AAR) is the interconversion of amino acids from one chiral form (the L-*laevo*- form) to a mixture of L- and D- (*dextro*) forms. This chemical

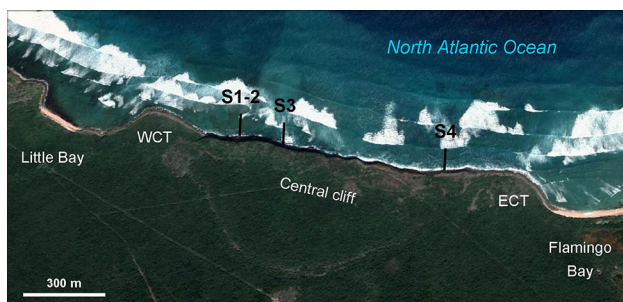


Fig. 3 Satellite image of the studied area. WCT western coral terrace; ECT eastern coral terrace. S sections. Image from Google Earth

reaction is a function of time and temperature, and can thus be used for geochronology. The extent of the epimerization (i.e. racemization) of L-isoleucine (I) to D-alloisoleucine (A), or A/I ratio, of our selected samples was measured (or calculated) at the Amino Acid Geochronology Laboratory of the Northern Arizona University. Up to four measurements were performed on each sample. Four whole-rock samples were analyzed in 2007 with the traditional ion exchange (IE) high-performance liquid chromatography (HPLC) method. Five additional samples were analyzed in 2018 with the innovative reverse-phase liquid chromatography (RPLC) technique (Kaufman and Manley 1998; Kaufman 2003) that allows to analyze submicroscopic samples (< 0.1 mg) such as single foraminifers. The RPLC technique determines the extent of racemization using primarily D/L glutamic (Glu) acid. For comparison with previous results obtained with the traditional IE-HPLC method yielding A/I values, D/L Glu values were converted to A/I using the equations established by Whitacre et al. (2017). The A/I ratio amounts to zero in modern sediments and increases to an equilibrium value of 1.3 for infinite-age rocks (Hearty and Kaufman 2000, 2009). Obtained A/I ratios were correlated with aminozones and marine isotope stages (MIS) following the directives of Hearty and Kaufman (2009). We have used both correlation charts proposed by these authors (Fig. 2a and b in Hearty and Kaufman 2009) that regrettably lead to slightly different interpretations. The application of the AAR-dating method to whole-rock samples is discussed in more detail in Hearty et al. (1992) and Hearty and Kaufman (2009).

X-ray diffraction (XRD) analysis was performed on eight samples with a Phillips PW 1710 diffractometer at the Institute of Geosciences of the University of Fribourg (Switzerland) to quantify the proportion of aragonite, calcite and gypsum. Diffractograms were recorded between 5° and 80° 2θ with the step-side mode. Quantitative Rietveld analyses (Bish and Post 1993) were made with the SIR-QUANT software (Taylor 1991).

3.3 Estimation of past relative sea levels (RSL)

Evaluating the height of ancient sea levels from preserved marine deposits is a challenging task due to the uncertainty pertaining to the paleo water-depth and to the amount of post-depositional karstic denudation. Take for example a 200 ka-old *A. palmata* reefal terrace culminating at 5 m above present sea level in a tectonically stable area. Because this coral species thrives in water depths between 1 and 5 m in the Caribbean today (Lighty et al. 1982; Woodroffe and Webster 2014), RSL elevation during formation of this fictive reef can be estimated at between 6 and 10 above modern datum. In addition, as ca. 10 m of

reefal terrace might have been lost due to post-depositional denudation (rate up to 50 mm/kyr; Mylroie and Mylroie 2017), the past RSL, in this example, could have been as high as +20 m. In this paper, we provide minimal estimates of ancient RSLs. In all cases, we chose the shallowest possible paleo depth (1 m in this example) and we used a denudation rate of 25 mm/kyr in our calculations, considering that, due to dryer climatic conditions, the dissolution rate of limestone in Mayaguana could be half of that in Guam, where Mylroie and Mylroie (2017) made their study.

4 Results

The studied exposure is an E-W trending, 1.5 km-long rocky coast along the northern shoreline of Mayaguana. It extends from the eastern end of a pocket beach called Little Bay (Fig. 3; N22°26.273', W73°03.289') to the western end of the Flamingo Bay strand plain (Fig. 3; N22°26.122', W73°02.359'). Its eastern and western portions are made of low (0.5 to 2 m), calcrete-capped *coral terraces* that lap on a *central cliff* (Fig. 4), whose elevation varies from ca. 4 m at both its eastern (N22°26.190, W73°02.520') and western (N22°26.264', W73°03.033') ends to a maximum of 13 m in its middle part (N22°26.250, W73°02.975'). This cliff is by far the highest coastal relief on Mayaguana, and matches in height those of some northern Bahamian islands (e.g. Eleuthera). It is bound on its ocean-facing edge by a *fossil fringing reef* up to 2.5 m high (Fig. 4). The cliff is partly covered by vegetated rockfall talus that facilitates the access to its highest portions, but partially covers its base (Fig. 4). It further shows two m-scale, *speleothem-rich caverns* (Fig. 4), the bottom of which respectively occurs at 2.5 and 6 m above present sea level. The deeply karstified and densely vegetated landward side of the central cliff slopes smoothly towards the South (Fig. 3).

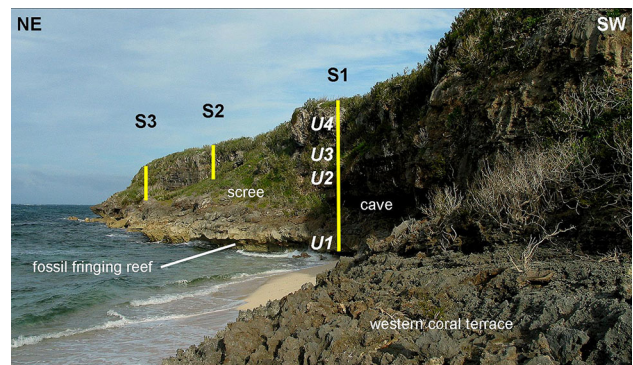


Fig. 4 Photograph of the western portion of central cliff at Misery Point showing the location of three of the four logged sections (S1 to S3). U stands for (stratigraphic) Units. Cliff height is about 13 m

4.1 Lithostratigraphy and sedimentology

4.1.1 The central cliff

We logged four detailed sections along the high portion of the Misery Point cliff: three of them near its highest point (Fig. 4; N22°26.250, W73°02.975'), and one near its eastern end (Fig. 3; N22°26.206, W73°02.711'). The cliff comprises four vertically stacked limestone units separated and capped by *terra-rossa* paleosols and/or erosional surfaces (Figs. 5 and 6a). All of these units can be observed on Sections 1 and 2, but their lower portion is variably covered by scree. Unit 2 is not visible at Section 3, possibly due to karst processes, and both Units 2 and 3 are missing at Section 4 (Fig. 5).

Unit 1 is a well-lithified bioclastic grainstone to floatstone containing numerous, dm-sized, partly dissolved mollusc (bivalves and gastropods) and coral debris (*Diploria strigosa*, *Acropora cervicornis*) which are particularly abundant in its middle portion. Isolated, m-scale coral colonies (*Diploria* sp.) also occur in this unit (Fig. 6b). The biocalcarenic matrix includes fragments of red and green algae, echinoids, benthic foraminifers (mostly miliolids and soritids), molluscs and corals. Cements are widespread and consist of fibrous rims, drusy fillings and rare menisci. A late gypsum cement (Fig. 7a) occludes both the primary and moldic porosities in the lower reaches of this unit, whereas the upper part shows numerous pedogenetic features (alveolar-septal structures, micritic zones, needle-

fiber calcite). All aragonitic components have been dissolved or replaced by calcite (Fig. 7a). The middle part of Unit 1 (between 3 and 5 m on Section 1) is characterized by the presence of large-scale, low-angle, seaward-dipping, planar cross stratifications, whereas its upper part shows low-amplitude, landward-dipping cross-bedding. Unit 1 is capped by a thick, penetrative *terra-rossa* paleosol (Fig. 6a). Its base occurs below sea level whereas its top reaches a maximum elevation of +7 m at Section 2 (Fig. 5). A minimal thickness of 7 m can thus be estimated for this unit. This succession was deposited in a peri-reefal setting, likely in a back-reef lagoon.

Unit 2 is a bioclastic rudstone to framestone rich in cm-sized pieces of corals (*A. cervicornis*, *Porites porites*, *Montastrea annularis*), branching red algae and gastropod shells (Figs. 6c and 7b). The rudstone/framestone matrix is a coarse porous grainstone to packstone with numerous encrusting and porcelaneous foraminifers bound by an early isopachous cement and a late drusy calcite mosaic (Fig. 7b). Some gypsum cement has also been observed in this lithology. The boundary with the overlying Unit 3 is sharp, but does not show evidence of pedogenesis or karstification (Fig. 6a). This lithology is exposed between +7 and +9 m on Section 1 and pinches out towards the East, being only 1 m thick on Section 2 and lacking on Sections 3 and 4 (Fig. 5). Unit 2 can be interpreted as an ancient low-energy reef (Geister, 1980). The facies of Units 1 and 2 are very similar to those of the pre-Lucayan limestone (Beach and Ginsburg 1980).

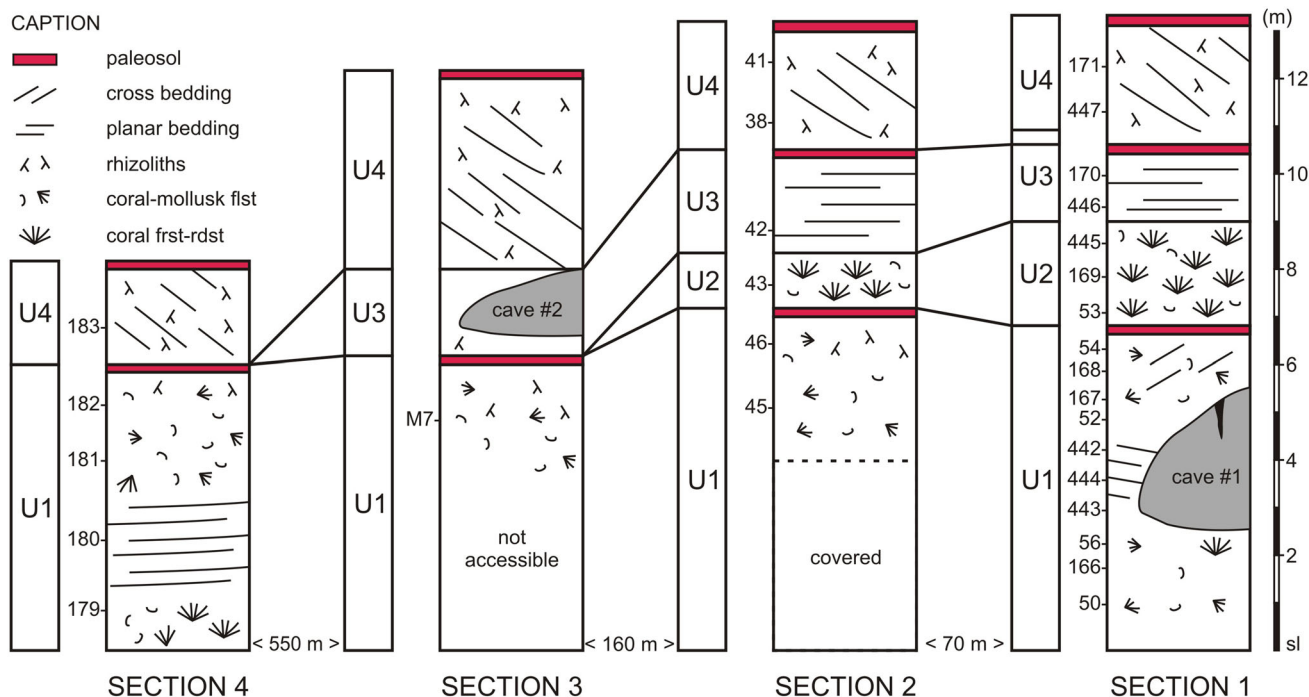


Fig. 5 Logs of stratigraphic sections from the central cliff. Numbers show the position of dated samples

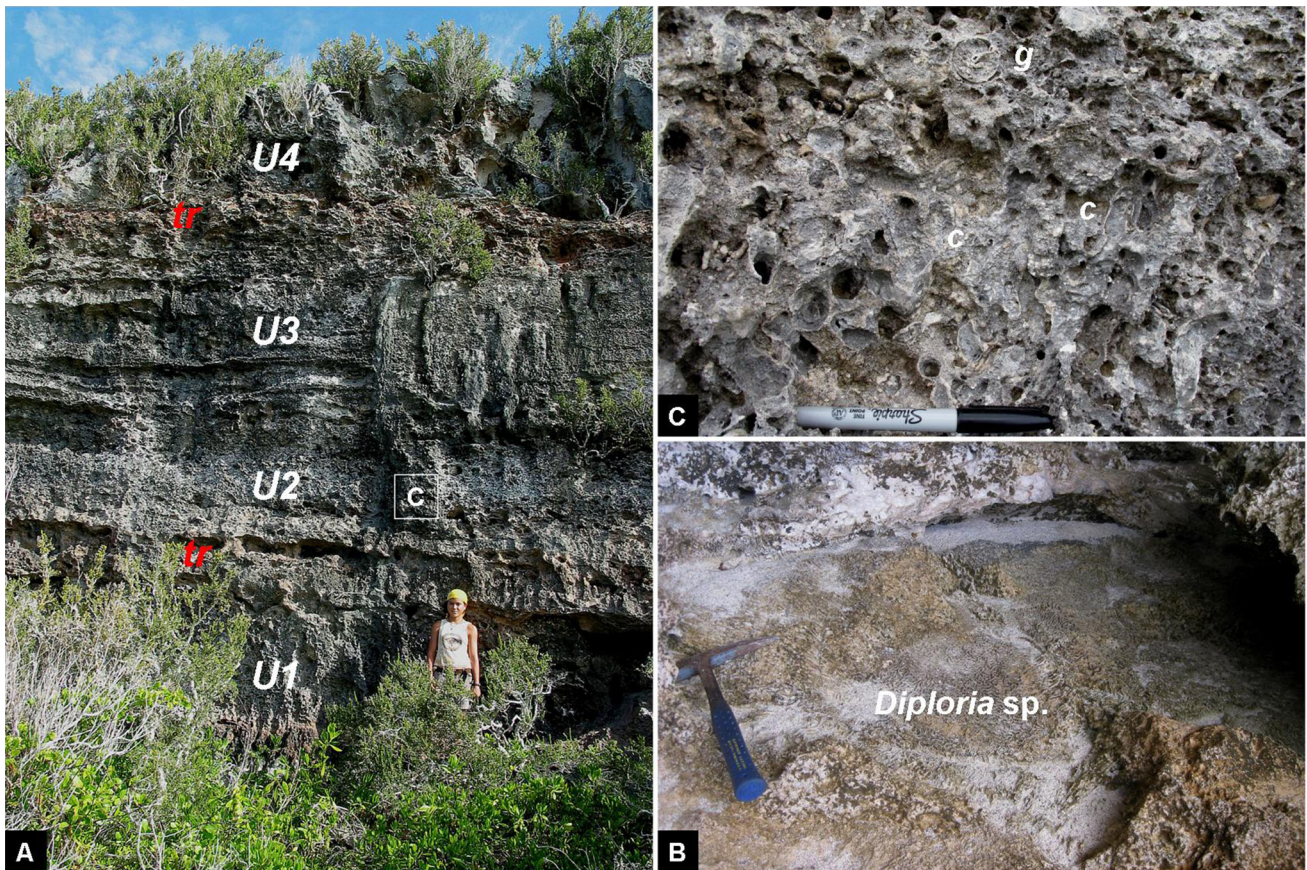


Fig. 6 **a** General view of Section 2. Note the occurrence of *terra-rossa* paleosols (*tr*) between U1 and U2, and U3 and U4. Note also well-marked planar bedding in U3. Letter C (in square) shows the location of Fig. 6c. Person for scale is 1.58 m tall. **b** m-scale *Diploria* sp. colony in U1 at Section 1. Hammer for scale is 36 cm long. **c** U2

reefal facies. Note numerous branches of possibly in situ *Acropora cervicornis* (c) and gastropod shell (g) in the rudstone/framestone matrix. Sample FAb 43 was collected at this location. Pen for scale is 15 cm long

Unit 3 is a well-lithified bioclastic grainstone characterized by well-marked planar cross-beds (Fig. 6a). In thin-section, it shows many fragments of encrusting and porcelaneous foraminifers as well as micro-oncoids (Fig. 7c), bound by two generations of cement: early fibrous rims and a late calcite mosaic (Fig. 7c). The top of this unit is affected by pedogenesis due to the presence of an overlying, thick *terra-rossa* paleosol (Fig. 6a). These rocks occur between +9 and +10.5 m on Section 1 and slightly thicken towards Section 2 because they fill the sloping topography of the underlying Unit 2 (Fig. 5). They are pervasively karstified on Section 3. The large-scale planar laminae, likely produced by wave swash, and the occurrence of fibrous marine cement, both indicate that Unit 3 represents fossil foreshore deposits. The occurrence of micro-oncoids in these calcarenites further shows this beach was probably facing a protected lagoon.

Forming the top of the cliff, Unit 4 is a relatively friable layer of well-sorted, skeletal calcarenite showing numerous calcified roots (Fig. 6a) and well-preserved, m-scale, cross-stratifications with a steep, landward dip. Bioclasts mostly

include fragments of molluscs, benthic foraminifers and green algae (*Halimeda* sp.) bound by meniscus calcite cement. Contrary to those of underlying units, aragonitic grains have occasionally preserved their original mineralogy (Fig. 7d). Pedogenetic features are widespread. The top of Unit 4 is deeply karstified and dissolution pits are filled by soil material. The maximum preserved thickness of this layer, visible on Section 3, is 5 m (Fig. 5). The large-scale foresets, numerous rhizoliths and meniscus cement identify this unit as an eolianite accumulated during fairly humid climatic conditions.

Several fan-shaped talus deposits front the central cliff at Misery Point. They almost reach up to the top of the cliff between Sections 1 and 2 (Fig. 4), and partly cover the base of Sections 2 and 3. They consist of a well-cemented, poorly sorted, clast-supported breccia with a locally reddish calcarenite matrix. Blocks display very irregular sizes (cm to m) and shapes, and consist of lithologies derived from Units 1–4 and of isolated coral fragments. These rockfall deposits both underlie and overlie the fossil fringing reef. They likely record several phases of cliff collapse.

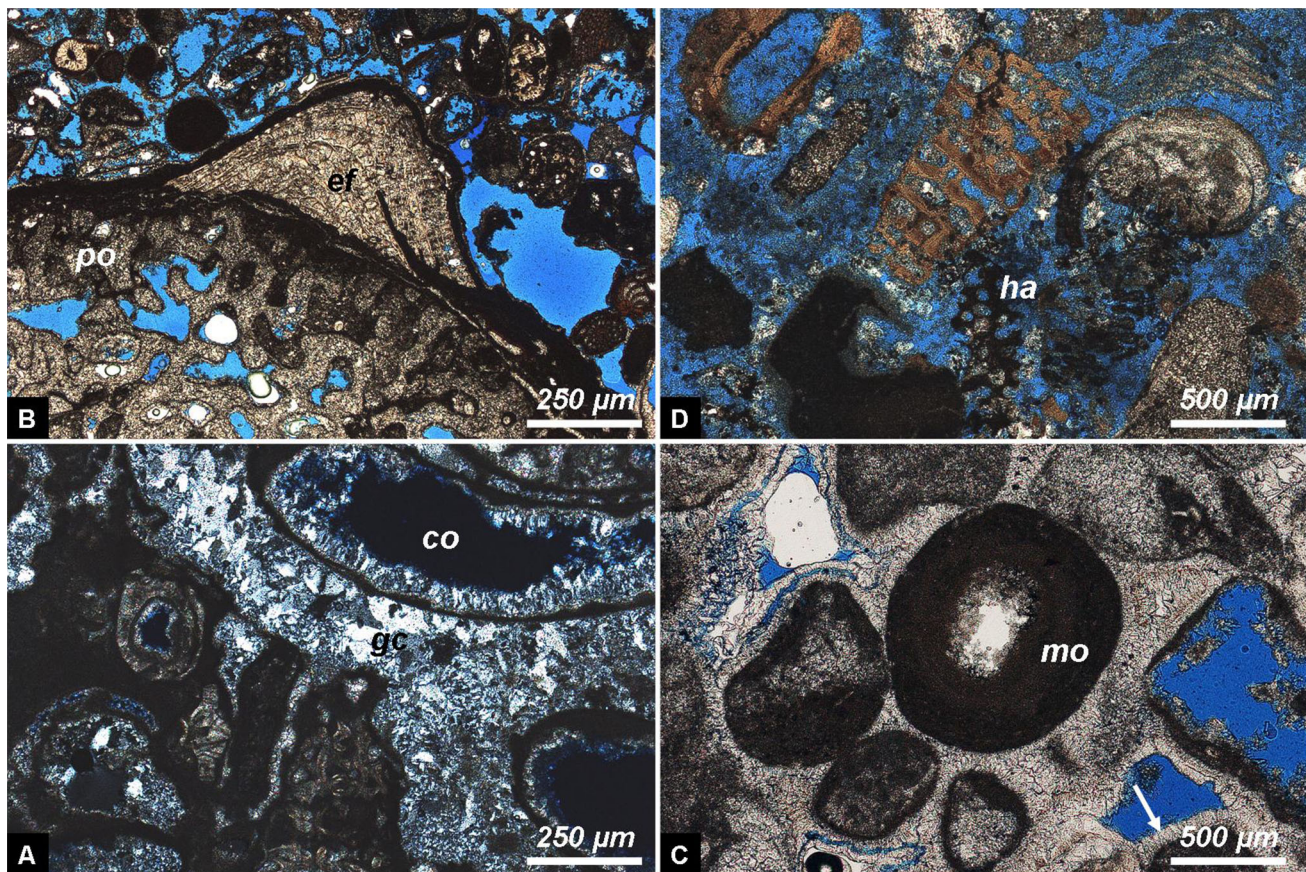


Fig. 7 Microfacies of stratigraphic units U1–U4. **a** Sample FAb 444 (cross-polarized light), Unit 1, Section 1. Biocalcarenic floatstone matrix. Note dissolved cortoids (*co*; i.e. rounded skeletal grains covered by a thin micritic envelope; Flügel 2004) and late gypsum cement (*gc*) filling both primary and secondary porosities. **b** Sample FAb 43 (plane-polarized light), Unit 2, Section 2. Bioclastic rudstone/framestone. Note large coral fragment (*po* = *Porites* sp.) encrusted by benthic foraminifer (*ef*), numerous dissolved cortoids in the rudstone/framestone matrix, and rare sparry cement. **c** Sample FAb 170 (plane-

polarized light), Unit 3, Section 1. Well-cemented grainstone. Note the occurrence of micro-oncoid (*mo*), and of a first generation of fibrous rim cement (arrow) indicating an early phase of marine diagenesis. **d** Sample FAb 171 (plane-polarized light), Unit 4, Section 1. Well-sorted, skeletal calcarenite. This portion of thin-section has been stained with Feigl's solution. The black stain on the *Halimeda* fragment (*ha*) reveals it has retained its original aragonite mineralogy. Note pedogenic micrite in primary porosity

4.1.2 The low-elevation coral terraces

The coral terraces bounding the high cliff to the West and East have a lateral extension of 0.4 and 0.3 km, respectively. Their elevation, and thus their minimal thickness, varies between 0.5 and 2 m above mean sea level, and their visible width (perpendicular to the shoreline) reaches up to 20 m. Landward, they are covered by recent storm rubble (Fig. 8a), whereas their seaward side is commonly marked by coastal karstic features (e.g. kamenizas). They consist of two superimposed lithologies: a coral framestone and an overlying, cm-thick, laminated, orange to red-brown, micritic crust (Fig. 8a). The massive coral framestone mostly comprises low-diversity colonies including *D. strigosa*, *M. annularis*, *M. cavernosa*, *M. nancyi* and *A. palmata*. The framestone matrix is a friable, somewhat pedogenized, bioclastic calcarenite rich in well-preserved porcelaneous and hyaline foraminifers. The coral

assemblage of these terraces is typical of a moderate-energy reef crest (Geister 1980). Considering the absence of an overlying paleosol, the micritic crust can be interpreted as a surficial calcrete (Wright 1994).

4.1.3 The fossil fringing reef

Unique on Mayaguana, this fossil reef fronts the high cliff and appears to both overlie and underlie the rock-fall deposits that locally mask it. Its lateral extent reaches about 20–30 m. Only accessible at low tide, it shows three vertically stacked facies (Fig. 8b). The basal one (0 to +1 m) predominantly includes massive *D. strigosa* framestone with a subordinate, mollusc-rich floatstone matrix. The diameter of the *Diploria* colonies ranges between 30 cm and 1 m. Laterally, smaller coral colonies occur, comprising species such as *Favia fragum*, *Agaricia agaricites* and *Manicina areolata*. All these corals, as well as the top

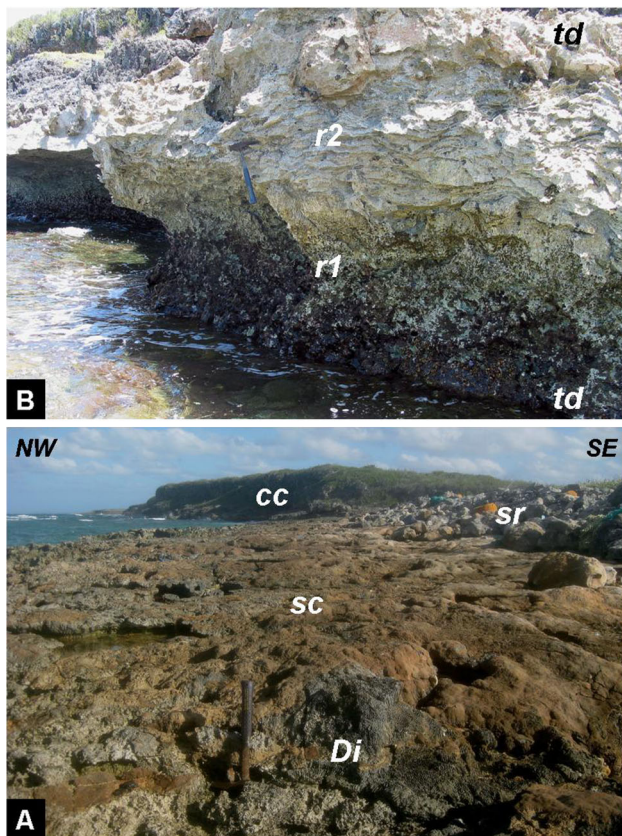


Fig. 8 **a** Field view of the western coral terrace looking towards the NE. *Di* = *Diploria* sp. colony; *sc* = surficial calcrete capping the coral framestone; *sr* = recent storm rampart; *cc* = central cliff. Hammer for scale is 36 cm long. **b** View of the fossil fringing reef at the base of the central cliff. *td* = talus deposits; *r1* = reef facies 1; *r2* = reef facies 2. Reef facies 3 is not visible on this picture. Same scale as in **a**

of this facies are encrusted by cm-thick red-algal crusts. About 1 m in thickness, the intermediate facies shows an alternation of cm-thick layers of encrusting corals (*D. clivosa* and *A. palmata*) and crustose coralline algae (Fig. 8b). The uppermost facies, exposed up to 2.5 m above sea level, comprises monogeneric coral colonies of *D. strigosa* and *D. clivosa*. The variable composition of this fringing reef indicates changing energy levels during its formation. The basal and the uppermost facies are typical of a moderately energetic setting, whereas the intermediate one reflects an increase in hydrodynamism.

4.2 Karstic features

The central cliff displays two remarkable, m-scale karstic cavities facing the open sea. The first one is carved in the upper part of Unit 1 at Section 1 (Fig. 9a). It forms one large, circular chamber, about 20 m in diameter from which radiate numerous smaller, subvertical and lateral conduits. Located at 2.5 m above sea level, the cave floor is

flat because it has been partly filled by recent sands (Fig. 9b). The maximum height of the cave reaches 3 m in its central part and pinches out laterally in all directions. The cave roof forms an undulating surface marked by numerous bell holes (Fig. 9b; Mylroie and Carew 1990) and is partially covered by flowstone (Fig. 9b). The cave further comprises a few stalactites, one flowstone column (Fig. 9a), a wave-cut notch at +3 m near its eastern end, and a small serpulid build-up close to its western entrance. The second cave affects Unit 3 at Section 3 (Fig. 9c and d). It is a notch-like feature about 15 m long, 2 m high, and 2 m deep. Its base is located at 6.5 m above modern sea level. The cave walls are partly covered by flowstone, and a few small stalactites are hanging from the roof. Based on the roof morphology and the occurrence of speleothems, these two features can be interpreted as the remnants of flank-margin (or probably halocline) caves opened by regressive erosion (Mylroie and Carew 1991; Mylroie and Mylroie 2017).

4.3 Geochronology

4.3.1 Sr-isotope data (Table 1)

$^{87}\text{Sr}/^{86}\text{Sr}$ ratios have been measured on 18 samples and subsamples collected from Unit 1 on Sections 1–4. Values range between 0.709114 and 0.709153. The average value amounts to 0.709128 ± 0.000011 . If we exclude two suspect outliers (FAB 180a and FAB 443), the average value amounts to 0.709126 ± 0.000009 . The four samples collected from Unit 2 on Sections 1 and 2 gave a mean ratio of 0.709131 ± 0.000006 . The four samples gathered from Unit 3 on Sections 1 and 2 provided values averaging at 0.709147 ± 0.000012 . However, if we eliminate one dubious outlier (FAB 170), the average value amounts to 0.709141 ± 0.000006 . Finally, 6 samples and subsamples collected from Unit 4 on Sections 1, 2 and 4 yielded values between 0.709149 and 0.709196. The sample which gave the highest value (FAB 183) has likely been contaminated by more radiogenic Sr from soil material, and is thus disregarded. Values from the five other samples average at 0.709153 ± 0.000006 .

4.3.2 U-series results (Table 2)

Six coral samples and one piece of speleothem were sent for U-series analysis. Calcitized fragments of *D. strigosa* (from Unit 1/Section 4) and of *A. cervicornis* (from Unit 2/Section 2) did not contain enough ^{238}U to yield reliable results, suggesting that their age is close to the limits of the U-series method (ca. 600 ka; Edwards et al. 2003). Nonetheless, a minimal age of 842.48 ka was calculated for the latter sample (FAB 43, Table 2). Fragments of *A.*

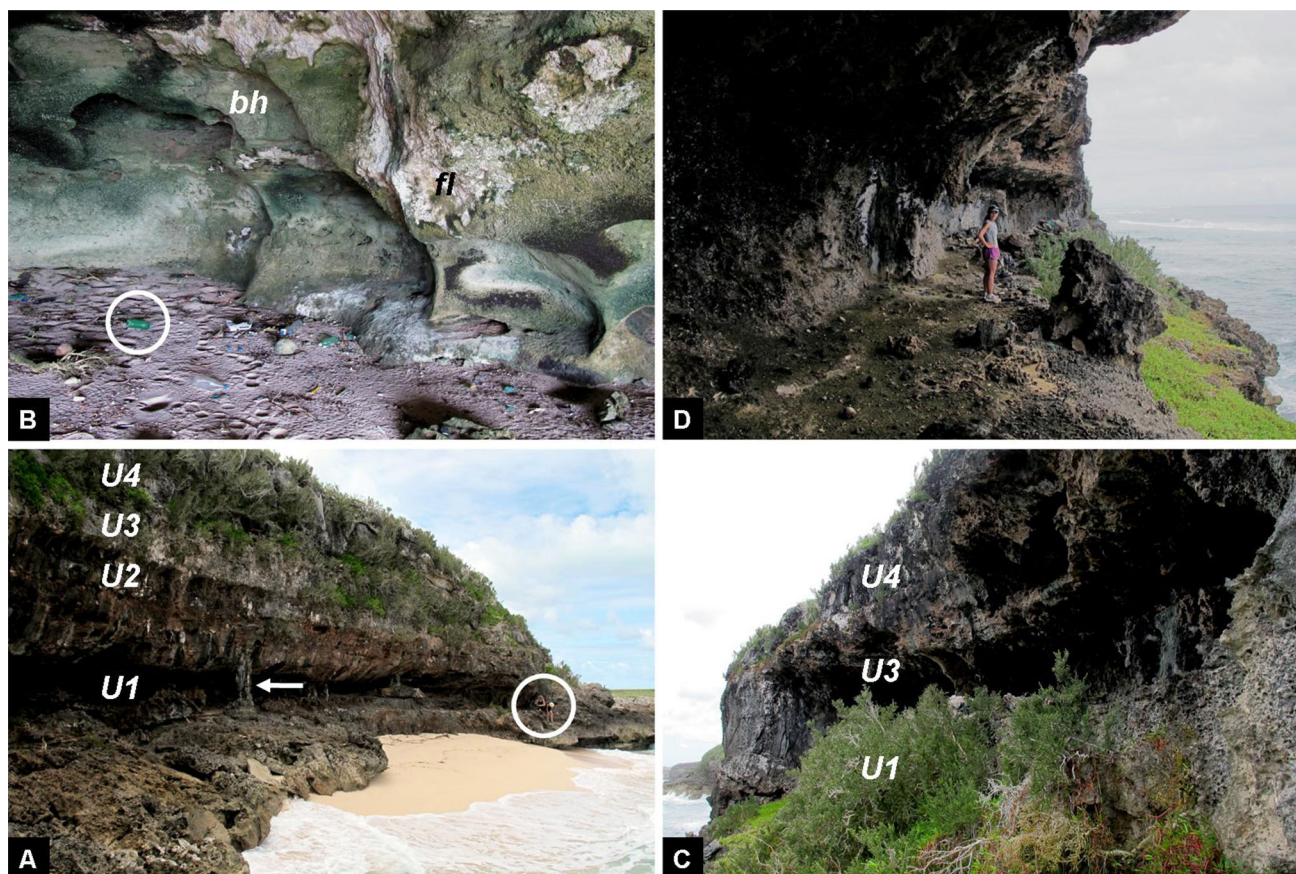


Fig. 9 Karstic features exposed on the central cliff at Misery Point. **a** View of the western part of the cave at Section 1. Note flowstone column (white arrow). Persons for scale (in white circle) are ca. 1.7 m tall. The cave is carved in the upper portion of Unit 1 (Fig. 5). **b** Cave interior at the same location. Note sand-covered floor, circular hollows in the ceiling named bell holes (*bh*; Mylroie and Carew 1990)

and flowstone drapes (*fl*) along the walls. Bottle (within circle) for scale is 20 cm long. **c** General view of the cave at Section 3 looking towards the E. The cave floor is located at +6.5 m above sea level. U1–4 = Units 1 to 4. **d** Same cave, looking towards the W. Note stalactite hanging from the ceiling behind the figure. Person for scale is 1.58 m tall

palmata and of *D. strigosa* from, respectively, the western and eastern terrace gave ages of ca. 125 and 123 ka BP. Specimens of *M. annularis* and of *D. clivosa*, collected respectively from the lower and the middle facies of the fossil fringing reef, gave ages of 123 and 122 ka BP. Finally, the core and the outer layer of one large stalactite hanging from the cave roof at Section 1 gave respective ages of 37 and 28 ka BP.

4.3.3 AAR data (Table 3)

A/I ratios were (1) measured on four samples collected from the central cliff and the low-elevation coral terrace (Table 3, upper portion), and (2) calculated from the measured D/L Glu ratios of five samples gathered from Units 1–4 at Sections 1 and 2 (Table 3, lower portion). Up to four measurements were performed per sample, but only the mean values are reported here.

Two samples collected from Unit 1 at Sections 1 and 2 gave A/I ratios of 0.518 ± 0.039 (measured) and

0.343 ± 0.006 (calculated), respectively. Two samples gathered from Units 2 and 3 at Section 2 gave calculated A/I values of 0.354 ± 0.035 and 0.767 ± 0.007 , respectively. One sample from Unit 4 at Section 2 yielded one measured A/I ratio of 0.418 ± 0.001 and one calculated value of 0.342 ± 0.027 , whereas one sample from the same unit at Section 1 gave a calculated value of 0.779 ± 0.001 . One sample from the serpulid boundstone located at the entrance of the flank-margin cave at Section 1 gave an A/I ratio of 0.372 ± 0.001 . Finally, one whole-rock sample from the framestone matrix of the western reefal terrace yielded an A/I value of 0.301 ± 0.001 .

5 Interpretation

We discuss below the age of the studied units, and the elevation and age of the observed sea-level indicators. We then provide a reconstruction of the evolution of the

Table 1 Sr-isotope dating results

Sample#	Unit	Sect.	$^{87}\text{Sr}/^{86}\text{Sr}$ measured	STD	$^{87}\text{Sr}/^{86}\text{Sr}$ normalized	STD
<i>FAb 183</i>	4	4	0.709217	0.000005	0.709196	0.000010
<i>FAb 38</i>	4	2	0.709139	0.000002	0.709145	0.000007
FAb 41	4	2	0.709173	0.000002	0.709158	0.000003
Fab 171b	4	1	0.709166	0.000001	0.709151	0.000002
<i>Fab 171a</i>	4	1	0.709181	0.000005	0.709160	0.000010
<i>FAb 447</i>	4	1	0.709151	0.000002	0.709149	0.000002
<i>FAb 42a</i>	3	2	0.709130	0.000003	0.709136	0.000007
FAb 42b	3	2	0.709163	0.000001	0.709148	0.000003
<i>FAb 446</i>	3	1	0.709142	0.000004	0.709140	0.000004
<i>FAb 170</i>	3	1	0.709184	0.000006	0.709164	0.000010
<i>FAb 43</i>	2	2	0.709120	0.000005	0.709126	0.000007
<i>FAb 53</i>	2	1	0.709120	0.000004	0.709126	0.000007
FAb 445	2	1	0.709152	0.000001	0.709137	0.000002
<i>FAb 169</i>	2	1	0.709156	0.000007	0.709136	0.000010
<i>FAb 181</i>	1	4	0.709095	0.000006	0.709120	0.000015
<i>FAb 180a</i>	1	4	0.709173	0.000008	0.709153	0.000010
FAb 180b	1	4	0.709158	0.000002	0.709143	0.000003
FAb 179b	1	4	0.709130	0.000002	0.709115	0.000003
<i>FAb 179a</i>	1	4	0.709141	0.000007	0.709121	0.000010
May 7	1	3	0.709130	0.000002	0.709114	0.000004
<i>FAb 46</i>	1	2	0.709117	0.000002	0.709123	0.000007
<i>FAb 45</i>	1	2	0.709118	0.000004	0.709124	0.000007
FAb 168b	1	1	0.709147	0.000001	0.709132	0.000002
<i>FAb 168a</i>	1	1	0.709162	0.000006	0.709141	0.000010
<i>FAb 167</i>	1	1	0.709156	0.000006	0.709136	0.000010
<i>FAb 442</i>	1	1	0.709120	0.000002	0.709118	0.000002
<i>FAb 443</i>	1	1	0.709146	0.000009	0.709144	0.000009
<i>FAb 444</i>	1	1	0.709130	0.000003	0.709128	0.000003
<i>FAb 56</i>	1	1	0.709111	0.000005	0.709117	0.000007
FAb 166b	1	1	0.709150	0.000002	0.709135	0.000004
<i>FAb 166a</i>	1	1	0.709143	0.000007	0.709122	0.000010
FAb 50	1	1	0.709141	0.000002	0.709126	0.000003

Normal characters: samples analysed in Geneva on a Thermo TRITON mass spectrometer. Italics: samples analysed in Kiel on a Nu instruments MC-ICPMS. Bold characters: samples analysed in Geneva on a Thermo Neptune PLUS Multi-Collector ICP-MS

Sct. section number, STD standard deviation

northern part of the Mayaguana platform during the Pleistocene.

5.1 Age of the studied units

5.1.1 The central cliff (Table 4)

We performed 26 Sr analyses on the marine beds (Units 1–3) forming the lower part of the central cliff at Misery

Point. This data base can be considered as significant which minimizes the uncertainties related to analytical errors (Table 1) and the imprecision pertaining to the establishment of the reference curve (Howarth and McArthur 1997; McArthur et al. 2001). These 26 measured values average at 0.709132 ± 0.000012 . Considering all possible errors and inexactness, this mean value corresponds to an age comprised between 1.308 and 0.814 Ma. Thus, Units 1 to 3 can confidently be assigned to the Early Pleistocene subepoch, more specifically to the late part of the Calabrian (Fig. 10; 1.806–0.781 Ma BP, Ogg and Pillans 2008). Nonetheless, we agree that magnetostratigraphy would be beneficial to reinforce this assumption (Units 1–3 should belong to the Matuyama Chron), although paleomagnetic studies performed up to now on eolianites and paleosols from the Bahamas obtained results that “have to be viewed with guarded optimism” (Panuska et al. 1995).

The average value of 0.709126 ± 0.000009 calculated for Unit 1 indicates an age between 1.348 and 1.016 Ma and between 1.228 and 1.150 Ma when disregarding the possible analytical error. The former time interval extends from MIS 43 to MIS 29 and the latter from MIS 37 to MIS 35 (Fig. 10). The mean ratio of 0.709131 ± 0.000006 obtained from Unit 2 corresponds to an age between 1.242 and 0.977 Ma and between 1.156 and 1.078 Ma if the potential analytical error is not considered. The former period stretches from MIS 37 to MIS 27, the latter from MIS 35 to MIS 31 (Fig. 10). The three reliable ratios measured on Unit 3 average at 0.709141 ± 0.000006 , thus indicating an age between 1.095 and 0.748 Ma or between 0.997 and 0.888 Ma if the potential analytical error is not considered. The former time interval encompasses MIS 32 to MIS 18, the latter MIS 28 to MIS 22 (Fig. 10). Finally, the values measured on the five reliable samples from Unit 4 average at 0.709153 ± 0.000006 , suggesting an age between 0.852 and 0.484 Ma and between 0.712 and 0.628 Ma when disregarding the possible analytical error. These time periods cover the intervals between MIS 22 and MIS 13 and between MIS 18 and 16, respectively (Fig. 10).

To sum up, the Sr data collected from the central cliff clearly show that the lower marine units (Units 1–3) are of Early Pleistocene age. Because a high sea level is needed to flood the Mayaguana bank and generate sediments, plotting the minimal age range obtained for each unit on Lisieki and Raymo’s (2005) $\delta^{18}\text{O}$ curve (a proxy for sea level) suggests that Unit 1, 2 and 3 could have been deposited during MIS 37 (~ 1.24 Ma BP), MIS 31 (~ 1.06 Ma BP) and MIS 25 (~ 0.94 Ma BP), respectively, and that Unit 4 accumulated during the early part of the Middle Pleistocene, possibly during MIS 17 (~ 0.68 Ma BP; Fig. 10). These estimates are consistent with those derived from a slightly different data base including also other exposures of similar rocks on Mayaguana (Kindler et al. 2011). Thus,

Table 2 U-series dating results

Sample (Fab)	Loc.	Co.	Calcite (%)	Age (ky)	± (ky)	²³⁸ U (ppm)	± (ppm)	²³² Th (ppb)	± (ppb)	²³⁰ Th/ ²³² Th (dpm/dpm)	±	²³⁰ Th/ ²³⁸ U (dpm/dpm)	±	²³⁴ U/ ²³⁸ U (dpm/dpm)	±	²³⁴ U/ ²³⁸ U init. (dpm/dpm)
43	CC2	A.c.	99.2	>842.48	n.d.	0.356	0.000	1.892	0.013	617	5	1.05801	0.00318	1.0344	0.0025	n.d.
48	FR1	M.a.	0.7	122.99	0.74	2.832	0.002	1.210	0.013	5491	61	0.75757	0.00087	1.1076	0.0010	1.5667
49	FR2	D.c.	1.7	122.28	0.58	2.698	0.002	1.258	0.014	5039	57	0.75920	0.00108	1.1065	0.0013	1.5683
52a	CC	spel.	100.0	24.75	2.04	0.193	0.000	43.840	0.095	3.38	0.02	0.24761	0.00119	1.0039	0.0012	1.0769
52b	CC	spel.	98.5	37.43	0.36	0.356	0.001	6.231	0.015	53.3	0.2	0.30146	0.00091	1.0258	0.0029	1.1407
175	WCT	A.p.	0.0	125.47	0.93	2.314	0.002	0.016	0.053	338724	101461	0.7676	0.0016	1.1070	0.0010	1.1520
182	CC1	D.s.	98.4	n.d.	n.d.	0.828	0.001	4.803	0.054	639	7.49	1.1973	0.0039	1.0370	0.0020	n.d.
184	ECT	D.s.	3.0	122.70	0.99	2.673	0.002	3.577	0.047	1746	23.21	0.7549	0.0020	1.1020	0.0010	1.1440

Loc. = sample location, CCx central cliff unit x, FRx fringing reef facies x, WCT Western coral terrace, ECT Eastern coral terrace, Co = sample type, A.c. *Acropora cervicornis*, M.a. *Montastrea annularis*, D.c. *Diploria clivosa*, D.s. *Diploria strigosa*, spel. speleothem, A.p. *Acropora palmata*

assuming these ages are acceptable, the time gaps between deposition of the stratigraphic units exposed on the central cliff can be evaluated at ~ 180 kyr (Units 2/1), ~ 120 kyr (Units 3/2) and ~ 260 kyr (Units 4/3; Fig. 10), respectively.

Except for one sample (FAB 171, Table 3) that yielded an age greater than 0.5 Ma for Unit 4 at Section 1, AAR analyses tell a different story. The sample collected from Unit 1 at Section 1 gave an A/I ratio (0.518) that can be correlated with aminozone E2 or F/G (Early MIS 5e or MIS 7; Table 3, Fig. 10). Moreover, four out of five results from Section 2 can be correlated with aminozones E1 or C indicating the Late Pleistocene (MIS 5e or 5a; Table 3, Fig. 10), but one sample (FAB 42), collected from the middle portion of the cliff (Unit 3), can be assigned to the lower part of the Middle Pleistocene (MIS 9 to > MIS 13; Table 3, Fig. 10).

We agree with the Sr-isotope results for the following reasons: (1) field observations show that the central cliff must predate the last interglacial because well-dated coral build-ups of this age lap on or border the cliff face (Fig. 4); (2) contrary to the AAR age estimates, all obtained Sr ages are in stratigraphic order; (3) the high diagenetic grade of the deposits, the low ²³⁸U content of the analysed coral fragments and the minimal age obtained on one of the coral samples collected from the central cliff (FAB 43, Table 2), all indicate an old age; (4) in the Bahamas region, the AAR method tends to provide anomalous results in rocks pre-dating the Middle Pleistocene (Hearty 2010); (5) in the Bahamas islands, MIS 5e deposits are predominantly composed of aragonitic ooids (Kindler and Hearty 1996), which is not the case of the sediments forming the central cliff.

5.1.2 Other features

The fossil fringing reef, the low-elevation coral terraces, the serpulid boundstone and the speleothem, all gave ages corresponding to the Late Pleistocene. The U-series analyses on the coral framestone ($n = 4$, Table 2) indicate a MIS 5e age (ca. 124 ka BP; Fig. 10), whereas the single AAR result on the framestone matrix (Table 3) correlates with MIS 5a (ca. 80 ka BP; Fig. 10). This discrepancy can be explained by the pedogenic alteration of the matrix that rejuvenated the A/I ratio (Brown 1985). However, this younger age could also be valid and indicate that the filling of the coral framestone porosity postdates its formation. These results are consistent with data obtained by Godefroid (2012) from similar fossil coral terraces along the Mayaguana shoreline. Based on AAR data, the serpulid boundstone located at the entrance of the flank-margin cave at Section 1 can be assigned to the early part of MIS 5e or to MIS 5a (aminozone E1 or C; Table 3, Fig. 10). We

Table 3 Amino-acid racemization dating results

Sample#	Unit	Sect.	A/I ratio measured	STD	Aminozone	MIS
FAb 174	CT	–	0.301	0.002	C	5a
FAb 172	SB	1	0.372	0.001	C–E1	5a–5e
FAb 38	4	2	0.418	0.001	E 1	Late 5e
FAb 56	1	1	0.518	0.039	E2 –F/G	5e–7
Sample #	Unit	Sect.	A/I ratio calculated	STD	Aminozone	MIS
FAb 171	4	1	0.779	0.001	I	>13
FAb 38	4	2	0.342	0.027	C	5a
FAb 42	3	2	0.767	0.007	H–I	9 ≥13
FAb 43	2	2	0.354	0.035	C–E1	5a–5e
FAb 45	1	2	0.343	0.006	C	5a

Upper portion of the table provides measured A/I ratios (IE-HPLC method); lower portion of the table gives calculated A/I ratios from measured D/L Glu values with the RPLC technique

Sect. Section number, STD standard deviation, MIS marine isotope stage, CT coral terrace, SB serpulid boundstone

exclude the latter possibility because the MIS 5a record in the Bahamas does not include marine deposits (Kindler and Hearty 1996). Finally, the core and the outer layer of the large stalactite hanging from the cave roof at Section 1 can be assigned to MIS 3 (Table 3, Fig. 10; 64–32 ka BP, Murray-Wallace and Woodroffe 2014).

5.2 Elevation and age of relative sea-level (RSL) indicators (Table 5)

As stated in the Sect. 3, we propose here minimal estimates for RSL elevations during deposition of the stratigraphic units exposed in the Misery Point area.

The moderate-energy, back-reef sediments of Unit 1 reach up to 7 m above present sea level. In the Bahamas, the depth of back-reef lagoons generally varies between 2 and 6 m (Bathurst 1975), and as much as 4.5 m of rocks might have been lost during the 180 kyr time gap between the deposition of Units 1 and 2. Knowing that part

of the dissolved beds could have been deposited in intertidal or supratidal settings, past RSL for Unit 1 (i.e. possibly during MIS 37) can be estimated between 9 and 13.5 m above modern datum.

The overlying, low-energy *A. cervicornis* reef of Unit 2 is exposed up to +9 m on the Misery Point cliff. *A. cervicornis* thrives at depths between 5 and 25 m today (Aronson and Precht 2001), and a ca. 3 m-thick carbonate layer could have been dissolved during the 120 kyr interval between the formation of Units 2 and 3. Because a significant portion of the dissolved strata could have accumulated in shallower settings (intertidal and/or supratidal), past RSL for Unit 2 (i.e. possibly during MIS 31) can be comprised +14 and +17 m.

The foreshore sediments of Unit 3 occur between 9 and 10.5 m above mean sea level. As the foreshore comprises the intertidal area, such deposits are a fairly precise indicator of past RSLs. About 6.5 m of carbonates could have been removed during the 260 kyr separating the deposition of Units 3 and 4. However, because these beach beds have about the same thickness (1–2 m) as counterparts observed in younger successions (e.g. Kindler and Hine 2009), denudation must have essentially removed backshore sediments. Consequently, the elevation of RSL during deposition of Unit 3 (i.e. possibly during MIS 25) can be estimated at about +10 m.

The eolian sediments of Unit 4 form the upper portion of the central cliff between +10.5 and +13 m and, based on the occurrence of numerous rhizoliths, were likely deposited during a humid period. Such climatic conditions favour vegetation and meteoric cementation which constrain eolianite deposition to a zone adjacent to the shoreline (Abegg et al. 2002). However, because Holocene dunes have been observed up to the elevation of 40 m in the Bahamas (e.g. Lee Stocking Island; Kindler 1992), we can only conclude that RSL was below +10 m during deposition of Unit 4 (i.e. possibly during MIS 17).

The mixed coral assemblage (*D. strigosa*, *A. palmata*, *Montastrea* sp.) of the low-elevation terraces at ca. +2.0 m likely thrived at a depth between 5 and 10 m (Braithwaite 2016). Denudation could have removed a ca. 3 m-thick

Table 4 Proposed age model for the units of the central cliff at Misery Point

Units	Setting	Samples (#)	⁸⁷ Sr/ ⁸⁶ Sr (average)	Mean age (Ma)	Maximum range		Minimum range		Preferred correlation
					(Ma)	MIS	(Ma)	MIS	
U4	Eolian	5	0.709153	0.668	0.852–0.484	22–13	0.712–0.628	18–16	MIS 17
U3	Beach	3	0.709141	0.943	1.095–0.748	32–18	0.997–0.888	28–22	MIS 25
U2	Reef	4	0.709131	1.116	1.242–0.977	37–27	1.156–1.078	35–31	MIS 31
U1	Lagoon	16	0.709126	1.190	1.348–1.016	43–29	1.228–1.150	37–35	MIS 37

Age interpretations for the lithologic units of the central cliff based on Sr-isotope data (Table 1). Rejected samples are not considered in these interpretations. See text for more explanations

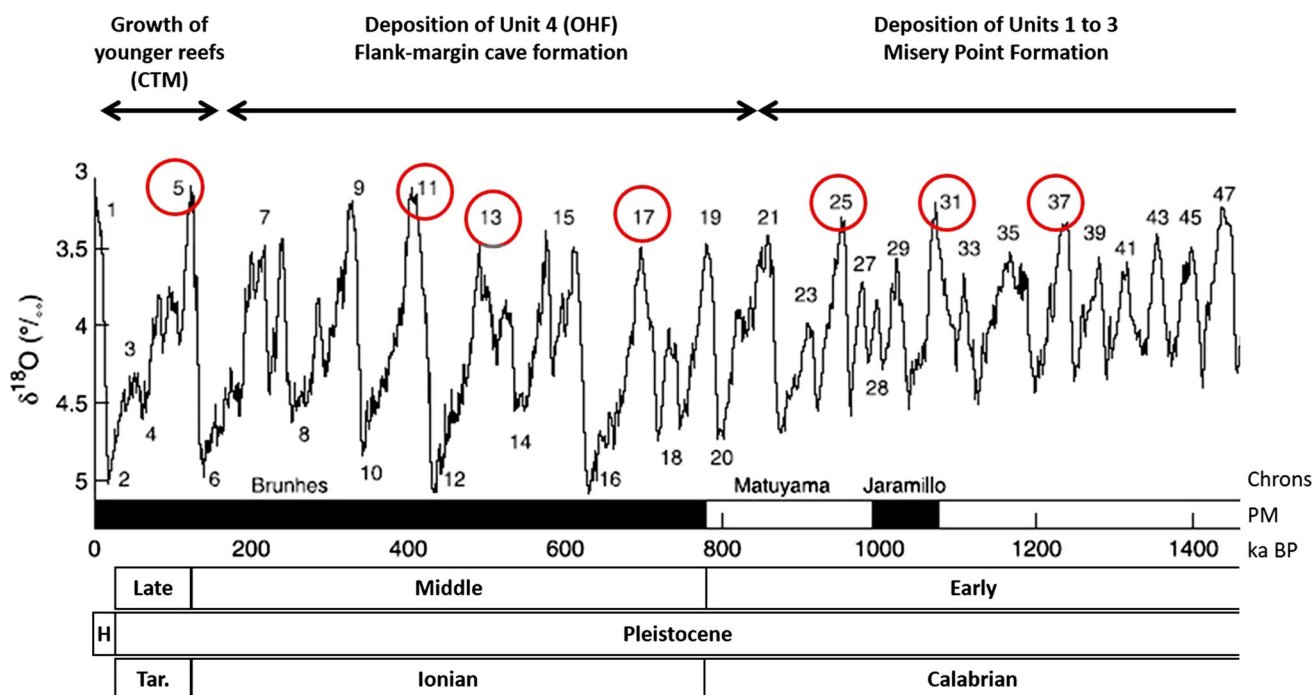


Fig. 10 Probable timing of depositional and erosional events at the Misery Point cliff, Mayaguana (red circles). Benthic oxygen-isotope curve is from Lisiecki and Raymo (2005); time scales in the lower part of the diagram are from Ogg and Pillans (2008). Abbreviations from

top to bottom: CTM = Cockburn Town Member; OHF = Owl's Hole Formation; PM = paleomagnetic record; H = Holocene; Tar. = Tarantian

Table 5 Age and elevation of RSL indicators at Misery Point

Units	Setting	Age (Ma)	MIS	RSL 1 m above msl	RSL 2 m above msl
CT	Reef	0.124	5	2	7–10
UC	Cave	?	? 11	8	8
LC	Cave	?	? 13	5	5
U4	Eolian	ca. 0.7	17	< 10	< 10
U3	Beach	ca. 0.9	25	9–10.5	ca. 10
U2	Reef	ca. 1.1	31	9	14–17
U1	Lagoon	ca. 1.2	37	7	9–13.5

Inferred age and elevation of past RSLs based on indicators observed at Misery Point

U1-4 units 1–4, *LC* lower flank-margin cave, *UC* upper flank-margin cave, *CT* coral terrace, *MIS* marine isotope stage, *RSL1* observed elevation of past RSL indicators; uncertainty is ± 0.2 m. *RSL2* relative elevation of past sea levels based on the elevation of RSL1, and considering the minimal paleo-depth of deposition and the amount of carbonate possibly removed by karstic denudation. In the case of caves, RSL2 = RSL1

carbonate layer since the last interglacial. As part of the dissolved beds could have been deposited in intertidal or supratidal settings, past RSL during the formation of these reefs (ca. 124 ka BP) can be estimated between 7 and 10 m above present. Finally, the peculiar faunal assemblage (alternation of encrusting corals and crustose red algae) within the fossil fringing reef at +2 m indicates an increase

in hydrodynamism that could possibly correspond to a m-scale lowering of the sea 122 ka ago.

Because they form at the distal end of fresh-water lenses, flank-margin caves are prime indicators of past sea levels (Myroie and Carew 1990, 1991; Myroie and Myroie 2017), but the timing of their formation is logically more difficult to constrain than that of sedimentary deposits. The cave exposed at Section 1 is carved in Unit 1, and its ceiling indicates a past RSL at ca. +5 m. The reentrant in Section 3 affects Unit 3, and its roof corresponds to a RSL slightly above +8 m. Although flank-margin caves can form fairly rapidly (in the order of 10 ka; Myroie and Carew 1990; Myroie and Myroie 2017), and even in the transgressive deposits predating a phase of stable sea level (*ibid.*), those visible at Misery Point likely postdate the Early Pleistocene because they occur at a lower elevation than the inferred RSLs for this time period (see previous section). Due to the presence of the serpulid bioherm of MIS 5e age near the entrance of the lower cave, their opening, due to regressive erosion or cliff collapse, likely occurred before the last interglacial. Thus, the karstic cavities carved in the central cliff were most probably formed during the sea-level highstands of the Middle Pleistocene (Fig. 10), possibly during MIS 13 (553–478 ka BP; Lisiecki and Raymo 2005), MIS 11 (424 to 374 ka BP; *ibid.*) and/or MIS 9 (337–300 ka BP; *ibid.*) when sea level was markedly higher than present (Hearty and Kindler

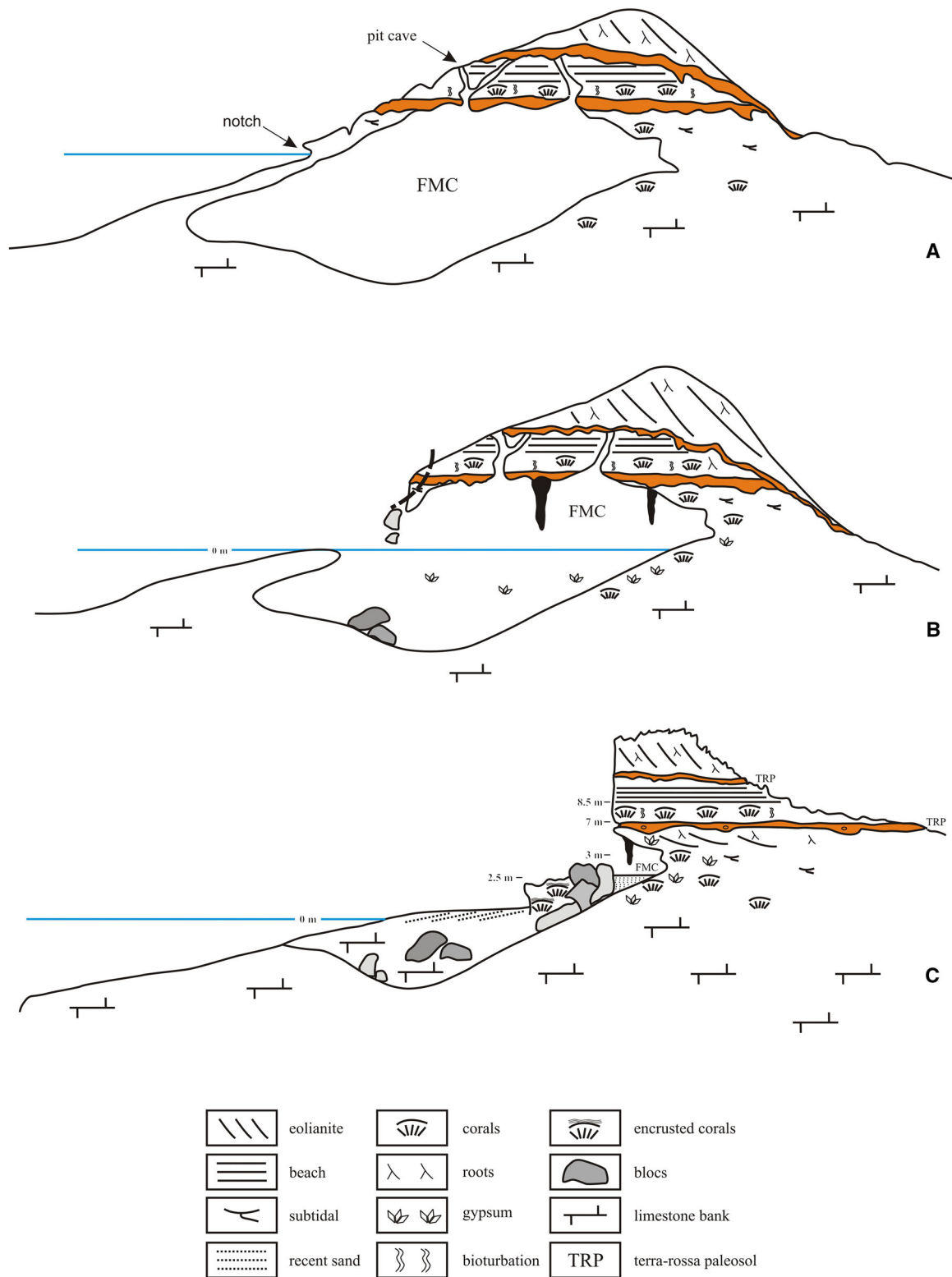


Fig. 11 Reconstruction of the Misery Point area from the Middle Pleistocene to the Present. **a** Late part of the Middle Pleistocene (MIS 13–9): Lower Pleistocene deposits are affected by pedogenic and karstic (cave formation) processes. FMC = flank-margin cave.

b Early part of the last interglacial. The cave has been opened and is flooded during the MIS 5e highstand leading to the formation of the serpulid bioherm. **c** Present-day situation. FMC = flank-margin cave. TRP = terra-rossa paleosols

1995; Hearty et al. 1999; Godefroid 2012). Finally, the wave-cut notch carved near the lower cave entrance at +3 m (Section 1) certainly postdates the cave opening, and is tentatively correlated with a phase of stable sea level during MIS 5e.

5.3 Geological history of the Misery Point area

The peri-reefal and reefal deposits of Units 1 and 2 show that, between ca. 1.24 Ma and 1.06 Ma (i.e. from MIS 37 to MIS 31) the Misery Point area, and possibly the entire Mayaguana bank, was covered by a ca. 5 m-deep water layer during sea-level highstands, and exposed during lowstands. The beach deposits of Unit 3 indicate that during MIS 25 (ca. 0.94 Ma ago), one low-elevation, sandy shoal formed behind a barrier reef in the Misery Point region. At that time, the platform was possibly similar to the present-day Cay Sal Bank (Hine and Steinmetz 1984), although the latter currently stands for the most part at a slightly greater depth. Shortly after the Early to Middle Pleistocene boundary (MIS 17; ca. 0.68 Ma ago), a larger and higher landform appeared in the area, as attested by the eolian facies of Unit 4. This “proto-Mayaguana” was likely one of the first highstand islands of the Bahamas, because the coeval rock records from the other Bahamian banks exclusively comprise marine sediments (Aurell et al. 1995; McNeill et al. 1998). Because of the stability of the Mayaguana bank, the modest sea-level events of the early part of the Middle Pleistocene (MIS 19 and 15) were unable to flood the platform, and thus did not leave any sedimentary record. During these highstands, the Misery Point area was a rocky islet only affected by pedogenic and karstification processes. The Mayaguana bank was likely submerged again in the later part of the Middle Pleistocene, as shown by the occurrence of reefal deposits of MIS 13 and MIS 11/9 age on Booby Cay (Godefroid 2012), and of a ca. 400 ka-old eolianite to the north of Abraham’s Bay (ibid.). No deposition took place near Misery Point at those times, possibly because of its high topography, but these highstands are likely recorded by the two flank-margin caves exposed in the central cliff (Figs. 9, 11a, b). The Mayaguana bank was largely flooded during the MIS 5e highstand which left an extensive record of subtidal, intertidal, and supratidal, mostly oolitic-peloidal sediments on the platform top, and numerous coral edifices on the margins, as at Misery Point (Fig. 11c). The last event to take place in the area was the formation of speleothems, possibly during a more humid interval in the latest Pleistocene.

6 Conclusions

We provided a detailed description of an exposure of skeletal carbonates (rudstones, framestones, floatstones and grainstones) of Early to Late Pleistocene age. The Lower Pleistocene (Upper Calabrian) portion of this outcrop has no equivalent elsewhere in the Bahamas islands. The following conclusions can be derived from our observations.

1. We present a reconstruction of the evolution of the Mayaguana bank during the past 1.25 million years, provide some insight on the birth of possibly the first highstand island of the Bahamas archipelago, and show that the northern margin of this bank, in the area of Misery Point, is largely erosional, because moderate- to low-energy deposits (Units 1–3) of Early Pleistocene age are now facing the open sea.
2. We show that the change in carbonate composition from skeletal to oolitic/peloidal (i.e. the switch from the pre-Lucayan to the Lucayan limestones; Beach and Ginsburg 1980) occurred much later on Mayaguana (after ca. 0.7 Ma ago) than in the subsurface of other Bahamian banks (between 3.6 and 2.6 Ma BP; McNeill et al. 1988, 1998; Manfrino and Ginsburg 2001). The reason for this difference remains for the moment uncertain. However, the younger occurrence of this change on Mayaguana suggests it is not uniquely related to the onset of northern-hemisphere glaciations (ca. 2.7 Ma ago; Hay 1992) as previously suggested by Beach and Ginsburg (1980).
3. The studied, km-scale outcrop shows a record of seven ancient sea-level highstands that occurred between ca. 1.25 Ma and 125 ka ago, and reached minimal relative elevations from 3 to 14 m above modern sea level. Considering the tectonic stability of the Mayaguana platform during the Quaternary, the amplitude of the recorded events could be fairly close to the corresponding eustatic changes, and thus provide calibration points for sea-level proxies derived from the deep-sea, oxygen-isotope record and further constrains to ice-sheet models.
4. Our study confirms the occurrence of high sea levels during the late part of the Calabrian (possibly during MIS 37, 31 and 25), but the amplitude of these events was of the same order of magnitude as the highstands of the Middle and of the Late Pleistocene.

Acknowledgements We thank F. Gischig (University of Geneva) for thin-section manufacturing, D.S. Kaufman, K. Whitacre and J. Bright (Northern Arizona University) for providing amino-acid racemization data, A. Eisenhauer and J. Fietzke (GEOMAR, Germany) for U-series dating, B. Grob ty (University of Fribourg) for XRD analyses, and M. Frank (GEOMAR, Germany) for some of the Sr-isotope results. Shorty, Tica and Tim are thanked for their logistical support on

Mayaguana. F. Prognon, C-A. Hasler, E. Samankassou and E. Baldessin's presence in the field was greatly appreciated. The patience of the Editors and the constructive comments from A. Strasser and two anonymous reviewers are acknowledged. Our expenses were supported by the Swiss National Science Foundation (Grant no. 200020-124608/1).

References

- Abegg, F. E., Loope, D. B., & Harris, P. M. (2002). Carbonate eolianites—depositional models and diagenesis. In F. E. Abegg, P. M. Harris, & D. B. Loope (Eds.), *Modern and ancient carbonate eolianites: sedimentology, sequence stratigraphy, and diagenesis* (pp. 17–30). Tulsa: SEPM Special Publication 71.
- Aronson, R. B., & Precht, W. F. (2001). White-band disease and the changing face of Caribbean coral reefs. *Hydrobiologia*, *460*, 25–38.
- Aurell, M., McNeill, D. F., Guyomard, T., & Kindler, P. (1995). Pleistocene shallowing-upward sequences in New Providence, Bahamas: signature of high-frequency sea-level fluctuations in shallow carbonate platforms. *Journal of Sedimentary Research*, *B65*, 170–182.
- Bathurst, R. G. C. (1975). *Carbonate sediments and their diagenesis* (p. 658). Amsterdam: Elsevier: Developments in Sedimentology 12.
- Beach, D. K., & Ginsburg, R. N. (1980). Facies succession of Pliocene–Pleistocene carbonates, Northwestern Great Bahama Bank. *American Association of Petroleum Geologists Bulletin*, *64*, 1634–1642.
- Bish, D. L., & Post, J. E. (1993). Quantitative mineralogical analysis using the Rietveld full-pattern fitting method. *American Mineralogist*, *78*, 932–940.
- Blanchon, P., Eisenhauer, A., Fietzke, J., & Liebetrau, V. (2009). Rapid sea-level rise and reef back-stepping at the close of the last interglacial highstand. *Nature*, *458*, 881–885.
- Braithwaite, C. J. R. (2016). Coral-reef records of Quaternary changes in climate and sea-level. *Earth-Science Reviews*, *156*, 137–154.
- Brown, R. H. (1985). Amino-acid dating. *Origins*, *12*, 8–25.
- Burckle, L. H. (1993). Late Quaternary interglacial stages warmer than present. *Quaternary Science Reviews*, *12*, 825–831.
- Camoin, G. F., Ebnen, P., Eisenhauer, A., Bard, E., & Faure, G. (2001). A 300'000-yr corals record of sea level changes, Mururoa atoll (Tuamotu archipelago, French Polynesia). *Paleogeography, Paleoclimatology, Paleocology*, *175*, 325–341.
- Cant, R.V. (1977). Role of coral deposits in building the margins of the Bahama Banks. In D. M. Taylor (Ed.), *Proceedings of the Third International Coral Reef Symposium* (Vol. 2, pp. 9–13), Miami.
- Carew, J. L., & Mylroie, J. E. (1995a). Depositional model and stratigraphy for the Quaternary geology of the Bahama Islands. In H. A. Curran & B. White (Eds.), *Terrestrial and shallow marine geology of the Bahamas and Bermuda* (pp. 5–32). Boulder: Geological Society of America Special Papers 300.
- Carew, J. L., & Mylroie, J. E. (1995b). Quaternary tectonic stability of the Bahamian archipelago: evidence from fossil coral reefs and flank margin caves. *Quaternary Science Reviews*, *14*, 145–153.
- DeConto, R. M., & Pollard, D. (2016). Contribution of Antarctica to past and future sea-level rise. *Nature*, *531*, 591–597.
- Edwards, R.L., Gallup, C.D., & Cheng, H. (2003). Uranium-series dating of marine and lacustrine carbonates. In B. Bourdon, G. M. Henderson, C. C. Lundstrom, S. P. Turner (Eds.), *Uranium-series geochemistry* (pp. 363–405). Reviews in Mineralogy and Geochemistry 52.
- Fietzke, J., Liebetrau, V., Eisenhauer, A., & Dullo, C. (2005). Determination of uranium isotope ratios by multi-static MIC-ICP-MS: method and implementation for precise U- and Th-series isotope measurements. *Journal of Analytical Atomic Spectrometry*, *20*, 395–401.
- Fischer G. (2019). Evolution of the Mayaguana Bank (SE Bahamas) since the earliest Miocene in the framework of tectonics and eustasy. *Ph.D. dissertation*, University of Geneva at Geneva, Switzerland.
- Fischer, G., Godefroid, F., Kindler, P., & Baldessin, E. (2016). Biostratigraphic and geochemical evidence for a tectonically induced change in the aggradation rate of the Mayaguana Bank (SE Bahamas) during the Early Miocene. In B. Glumac & M. Savarese (Eds.), *Proceedings of the 16th Symposium on the Geology of the Bahamas and other carbonate regions* (pp. 1–12). San Salvador, Bahamas: Gerace Research Center.
- Flügel, E. (2004). *Microfacies of carbonate rocks* (p. 976). Berlin: Springer.
- Geister, J. (1980). Calm-water reefs and rough-water reefs of the Caribbean Pleistocene. *Acta Palaeontologica Polonica*, *25*, 541–556.
- Godefroid, F. (2012). Géologie de Mayaguana, SE de l'archipel des Bahamas. *Ph.D. dissertation*, University of Geneva at Geneva, Switzerland, p. 230.
- Gvirtzman, G. (1994). Fluctuations of sea level during the past 400,000 years: the record of Sinai, Egypt (northern Red Sea). *Coral Reefs*, *13*, 203–214.
- Hay, W. W. (1992). The cause of the Late Cenozoic Northern Hemisphere glaciations: a climate enigma. *Terra Nova*, *4*, 305–311.
- Hearty, P. J. (2010). Chronostratigraphy and morphological changes in *Cerion* land snail shells over the past 130 ka on Long Island, Bahamas. *Quaternary Geochronology*, *5*, 50–64.
- Hearty, P. J., & Kaufman, D. S. (2000). Whole-rock aminostratigraphy and Quaternary sea-level history of the Bahamas. *Quaternary Research*, *54*, 163–173.
- Hearty, P. J., & Kaufman, D. S. (2009). A *Cerion*-based chronostratigraphy and age model from the central Bahama Islands: amino-acid racemization and ¹⁴C in land snails and sediments. *Quaternary Geochronology*, *4*, 148–159.
- Hearty, P. J., & Kindler, P. (1995). Sea-level highstand chronology from stable carbonate platforms (Bermuda and The Bahamas). *Journal of Coastal Research*, *11*, 675–689.
- Hearty, P. J., Kindler, P., Cheng, H., & Edwards, L. (1999). A +20 m middle Pleistocene sea-level highstand (Bermuda and The Bahamas) due to partial collapse of Antarctic ice. *Geology*, *27*, 375–378.
- Hearty, P. J., & Tormey, B. R. (2017). Sea-level change and superstorms; geologic evidence from the last interglacial (MIS 5e) in the Bahamas and Bermuda offers ominous prospects for a warming earth. *Marine Geology*, *390*, 347–365.
- Hearty, P. J., Vacher, H. L., & Mitterer, R. M. (1992). Aminostratigraphy and ages of Pleistocene limestones of Bermuda. *Geological Society of America Bulletin*, *104*, 471–480.
- Hine, A. C., & Steinmetz, J. C. (1984). Cay Sal Bank, Bahamas—a partially drowned carbonate platform. *Marine Geology*, *59*, 135–164.
- Horwitz, E. P., Chiarizia, R., & Dietz, M. L. (1992). A novel strontium-selective extraction chromatographic resin. *Solvent Extraction and Ion Exchange*, *10*, 313–336.
- Howarth, R. J., & McArthur, J. M. (1997). Statistics for strontium isotope stratigraphy. A robust LOWESS fit to the marine Sr-isotope curve for 0–206 Ma, with look-up table for the derivation of numerical age. *Journal of Geology*, *105*, 441–456.

- Kaufman, D. S. (2003). Amino acid paleothermometry of Quaternary ostracodes from the Bonneville Basin, Utah. *Quaternary Science Reviews*, 22, 899–914.
- Kaufman, D. S., & Manley, W. F. (1998). A new procedure for determining DL amino acid ratios in fossils using reverse phase liquid chromatography. *Quaternary Science Reviews*, 17, 987–1000.
- Kenter, J.A.M., Ginsburg, R.N., & Troelstra, S.R. (2001). Sea-level-driven sedimentation patterns on the slope and margin. In: R.N. Ginsburg (Ed.), *Subsurface geology of a prograding carbonate platform margin, Great Bahama Bank: results of the Bahamas Drilling Project* (pp. 61–100). Tulsa: SEPM Special Publication 70.
- Kindler, P. (1992). Coastal response to the Holocene transgression in the Bahamas: episodic sedimentation versus continuous sea-level rise. *Sedimentary Geology*, 80, 319–329.
- Kindler, P., Godefroid, F., Chiaradia, M., Ehlert, C., Eisenhauer, A., Frank, M., et al. (2011). Discovery of Miocene to early Pleistocene deposits on Mayaguana, Bahamas: evidence for recent active tectonism on the North American margin. *Geology*, 39, 523–526.
- Kindler, P., Godefroid, F., & Samankassou, E. (2008). Pre-Holocene island geology of the Caicos and Mayaguana (Bahamas) platforms: similarities and differences. In W. A. Morgan & P. M. Harris (Eds.), *Developing models and analogs for isolated carbonate platforms—Holocene and Pleistocene carbonates of Caicos Platform, British West Indies* (pp. 211–213). Tulsa: SEPM Core Workshop 22.
- Kindler, P., & Hearty, P. J. (1996). Carbonate petrography as an indicator of climate and sea-level changes: new data from Bahamian Quaternary units. *Sedimentology*, 43, 381–399.
- Kindler, P., & Hine, A. C. (2009). The paradoxical occurrence of oolitic limestone on the eastern islands of Great Bahama Bank: where do the ooids come from? In P. K. Swart, G. P. Eberli, & J. A. McKenzie (Eds.), *Perspectives in carbonate geology. A tribute to the career of Robert Nathan Ginsburg* (pp. 113–122). Chichester: IAS Special Publication 41.
- Kindler, P., Mylroie, J. E., Curran, H. A., Carew, J. L., Gamble, D. W., Rothfus, T. A., Savarese, M., & Sealey, N. E. (2010). Geology of Central Eleuthera, Bahamas: a field trip guide. In *Fieldtrip guidebook, 15th Symposium on the Geology of the Bahamas and other carbonate regions* (p. 75). San Salvador, Bahamas: Gerace Research Centre.
- Lighty, R. G., Macintyre, I. G., & Stuckenrath, R. (1982). Acropora Palmata reef framework: a reliable indicator of sea level in the Western Atlantic for the past 10,000 years. *Coral Reefs*, 1, 125–130.
- Lisiecki, L.E., & Raymo, M.E. (2005). A Pliocene-Pleistocene stack of 57 globally distributed benthic $\delta^{18}\text{O}$ records. *Paleoceanography*, 20, PA 1003, 1–17.
- Manfrino, C., & Ginsburg, R.N. (2001). Pliocene to Pleistocene depositional history of the upper platform margin. In: R.N. Ginsburg (Ed.), *Subsurface geology of a prograding carbonate platform margin, Great Bahama Bank: results of the Bahamas Drilling Project* (pp. 17–39). Tulsa: SEPM Special Publication 70.
- McArthur, J. M., Howarth, R. J., & Bailey, T. R. (2001). Strontium isotope stratigraphy: LOWESS Version 3. Best-fit line to the marine Sr-isotope curve for 0 to 509 Ma and accompanying look-up table for deriving numerical age. *Journal of Geology*, 109, 155–169.
- McNeill, D. F., Ginsburg, R. N., Chang, S.-B. R., & Kirschvink, J. L. (1988). Magnetostratigraphic dating of shallow-water carbonates from San Salvador, Bahamas. *Geology*, 16, 8–12.
- McNeill, D. F., Grammer, G. M., & Williams, S. C. (1998). A 5 My chronology of carbonate platform margin aggradation, Southwestern Little Bahama Bank, Bahamas. *Journal of Sedimentary Research*, 68, 603–614.
- Mesolella, K. J., Matthews, R. K., Broecker, W. S., & Thurber, D. L. (1969). The astronomical theory of climatic change: Barbados data. *Journal of Geology*, 77, 250–274.
- Meyerhoff, A. A., & Hatten, C. W. (1974). Bahamas salient of North America: tectonic framework, stratigraphy and petroleum potential. *American Association of Petroleum Geologists Bulletin*, 58, 1201–1239.
- Miller, K. G., Kominz, M. A., Browning, J. V., Wright, J. D., Mountain, G. S., Katz, M. E., et al. (2005). The Phanerozoic record of global sea-level change. *Science*, 310, 1293–1298.
- Mullins, H. T., & Lynts, G. W. (1977). Origin of the northwestern Bahama platform: review and reinterpretation. *Geological Society of America Bulletin*, 88, 1447–1461.
- Murray-Wallace, C. V. (2002). Pleistocene coastal stratigraphy, sea-level highstands and neotectonism of the southern Australian passive continental margin—a review. *Journal of Quaternary Science*, 17, 469–489.
- Murray-Wallace, C. V., & Woodroffe, C. D. (2014). *Quaternary sea-level changes. A global perspective* (p. 484). Cambridge: Cambridge University Press.
- Mylroie, J. E., & Carew, J. L. (1990). The flank margin model for dissolution cave development in carbonate platforms. *Earth Surface Processes and Landforms*, 15, 413–424.
- Mylroie, J.E., & Carew, J.L. (1991). Erosional notches in Bahamian carbonates: bioerosion or groundwater dissolution? In: R. J. Bain (Ed.), *Proceedings of the Fifth Symposium on the Geology of the Bahamas* (pp. 185–191). San Salvador, Bahamas: Bahamian Field Station.
- Mylroie, J. E., & Mylroie, J. R. (2017). Role of karst denudation on the accurate assessment of glacio-eustasy and tectonic uplift on carbonate coasts. In M. Parise, F. Gabrovsek, G. Kaufmann, & N. Ravbar (Eds.), *Advances in karst research: theory, fieldwork and applications* (pp. 171–186). London: Geological Society Special Publications 466.
- Neumann, A. C., & Hearty, P. J. (1996). Rapid sea-level changes at the close of the last interglacial (substage 5e) recorded in Bahamian island geology. *Geology*, 24, 775–778.
- O’Leary, M. J., Hearty, P. J., Thompson, W. G., Raymo, M. E., Mitrovica, J. X., & Webster, J. M. (2013). Ice sheet collapse following a prolonged period of stable sea level during the last interglacial. *Nature Geoscience*. <https://doi.org/10.1038/ngeo1890>.
- Ogg, J. G., & Pillans, B. (2008). Establishing Quaternary as a formal international period/system. *Episodes*, 31, 230–233.
- Panuska, B.C., Mylroie, J.E., Kirkova, J.T., & Carew, J.L. (1995). Correlation of paleosols on San Salvador Island using paleomagnetic directions. In: M. Boardman (Ed.), *Proceedings of the Seventh Symposium on the Geology of The Bahamas* (pp. 82–88). San Salvador, Bahamas: Bahamian Field Station.
- Pedoja, K., Husson, L., Johnson, M. E., Melnick, D., Witt, C., Pochat, S., et al. (2014). Coastal staircase sequences reflecting sea-level oscillations and tectonic uplift during the Quaternary and Neogene. *Earth-Science Reviews*, 132, 13–38.
- Pierson, B.J. (1982) Cyclic sedimentation, limestone diagenesis and dolomitization in upper Cenozoic carbonates of the southeastern Bahamas. *Ph.D. dissertation*. University of Miami at Miami, Florida, USA, pp. 286.
- Pirazzoli, P. A., Radtke, U., Hantoro, W. S., Jouannic, C., Hoang, C. T., Causse, C., et al. (1993). A one million-year-long sequence of marine terraces on Sumba Island, Indonesia. *Marine Geology*, 109, 221–236.
- Pollard, D., & DeConto, R. M. (2009). Modelling West Antarctic ice sheet growth and collapse through the past five million years. *Nature*, 458, 329–333.

- Raymo, M. E., Lisiecki, L. E., & Nisancioglu, K. H. (2006). Plio-Pleistocene ice volume, Antarctic climate, and the global $\delta^{18}\text{O}$ record. *Science*, *313*, 492–495.
- Scherer, R., Bohaty, S., Harwood, D., Roberts, A., & Taviani, M. (2003). Marine isotope stage 31 (1.07 Ma) an extreme interglacial in the Antarctic nearshore zone. *Geophysical Research Abstracts*, *5*, 11710.
- Speed, R.C. (2012). *Geology and geomorphology of Barbados* (p. 62). In C. Speed & R. Sedlock (Eds.). Boulder: Geological Special Paper 491.
- Supko, P. R. (1977). Subsurface dolomites, San Salvador, Bahamas. *Journal of Sedimentary Petrology*, *47*, 1063–1077.
- Taylor, J. C. (1991). Computer program for standardless quantitative analysis of minerals using the full powder diffraction profile. *Powder Diffraction*, *6*, 2–9.
- Thompson, W. G., Curran, H. A., Wilson, M. A., & White, B. (2011). Sea-level oscillations during the last interglacial highstand recorded by Bahamas corals. *Nature Geoscience*, *4*, 684–687.
- Thompson, W. G., & Goldstein, S. L. (2005). Open-system coral ages reveal persistent suborbital sea-level cycles. *Science*, *308*, 401–404.
- Whitacre, K., Kaufman, D. S., Kosnik, M. A., & Hearty, P. J. (2017). Converting A/I values (ion exchange) to D/L values (reverse phase) for amino acid geochronology. *Quaternary Geochronology*, *37*, 1–6.
- Woodroffe, C. D., & Webster, J. D. (2014). Coral reefs and sea-level change. *Marine Geology*, *352*, 248–267.
- Wright, V. P. (1994). Paleosols in shallow marine carbonate sequences. *Earth Science Reviews*, *35*, 367–395.